Supplementary Information for

Synergistic Defect Engineering and Interfacial Regulation in Amphiphilic Cerium-Based Metal–Organic Frameworks for Efficient Heavy Oil Upgrading

This PDF file includes:

Supplementary Methods

Supplementary Figures

Supplementary Tables

Supplementary Methods

Reagents and Materials

All metal precursors and organic reagents were purchased from Aladdin Biochemical Technology Co., Ltd. (Shanghai, China) with a minimum analytical purity of 99%. The main chemicals used include 2-aminoterephthalic acid ($C_3H_7NO_4$), ammonium cerium(IV) nitrate ($(NH_4)_2Ce(NO_3)_6$), 2-acrylamido-2-methylpropanesulfonic acid (AMPS, $C_7H_{13}NO_4S$), α-olefin sulfonate sodium (AOES, R1-CH=CH-(CH_2)n-SO_3Na, R1=C_9–C_{13}), acrylic acid (AA, $C_3H_4O_2$), sodium bisulfite, sodium persulfate, and sodium hydroxide. The organic solvents employed, including N,N-dimethylformamide (DMF, anhydrous), ethylene glycol (HPLC grade), hydrochloric acid, and absolute ethanol, were also obtained from the same supplier. All reagents and solvents were used as received without further purification.

The heavy crude oil used in this study was sourced from the Yuqi Block of the Tahe Oilfield in the Tarim Basin, Northwest China. Prior to experimentation, the crude oil underwent dehydration treatment, resulting in a water content below 0.5%. Rheological measurements indicated that the initial dynamic viscosity was 35,292 ± 1,250 mPa·s at 50°C.

Catalyst recycling, deactivation evaluation and regeneration protocol

To evaluate catalyst deactivation and regeneration behavior, each recycling experiment was conducted using fresh heavy oil, fresh connate water, and fresh tetralin as reactants, while the catalyst recovered from the previous run was reused in the subsequent cycle. After each reaction, the system was cooled to room temperature and centrifuged at 10,000 rpm for 15 min to achieve demulsification and solid–liquid separation, and the recovered catalyst solids were collected. The spent catalyst was then sequentially washed with toluene and ethanol to remove surface-adsorbed oil, soluble organic species, and weakly bound organic residues, respectively, followed by vacuum drying at 60ºC for 12 h. Prior to reuse, the catalyst was ultrasonically re-dispersed in fresh connate water. The relative activity retention of the catalyst was defined as the ratio of the viscosity reduction rate in the *n* th cycle to that in the first cycle. To probe the evolution of active sites and structural changes before and after reaction, fresh, spent, and regenerated catalysts were characterized by XPS (Ce 3d), XRD, Fourier transform infrared spectroscopy (FTIR), scanning electron microscopy (SEM), and transmission electron microscopy (TEM).

Characterization

The synthesized materials were systematically characterized using advanced analytical techniques: Morphological features were resolved via field-emission SEM (Zeiss Gemini 300, 5 kV) and high-resolution TEM (FEI-TALOS-F200X, 200 kV) with selected-area electron diffraction. Crystalline phases were identified by XRD (Bruker D8 Advance, Cu-Kα, λ=1.54056 Å) across 5-80° 2θ at 5°/min. Surface chemistry evolution was tracked through in situ XPS (Thermo Scientific K-Alpha+, Al-Kα, 1486.6 eV) under reductive 5% H_2/Ar atmosphere (200-400°C), with charge correction referenced to C 1s (284.8 eV). Molecular fingerprints were acquired by FTIR spectroscopy (Bruker Vertex 70, KBr pellets, 4000-400 cm^{-1}) and Raman microscopy (Renishaw inVia, 532 nm laser, 1 mW). Thermal stability was assessed via synchronous TGA-DSC (NETZSCH STA 449 F3, Ar, 10°C/min to 800°C). Porosity characteristics were quantified through N_2 physisorption (Micromeritics ASAP 2460, 77 K) following 6 h degassing at 300°C, with BET surface area and pore distributions (HK/BJH models) calculated from adsorption isotherms. Molecular structure verification included ^{1}H NMR spectroscopy (Bruker Avance III 400 MHz, $CDCl_3$/TMS, 32 scans) and GC-MS analysis (Agilent 7890B/5977A, DB-5MS column, 5°C/min ramp). This multiscale characterization protocol ensures comprehensive correlation between material architecture and functional performance.

Interfacial Properties of Catalysts and Mass Transfer Behavior in Reservoirs

This study employs a combination of multiscale interfacial characterization techniques and high-temperature, high-pressure dynamic simulation experiments to elucidate the interfacial regulation mechanisms of catalysts and their effects on mass transfer processes within reservoirs. Surface and interfacial tension evolution of catalyst solutions (0.1–1.0 wt%) are quantitatively measured using an automated tensiometer, while wettability alteration of sandstone substrates is assessed via contact angle measurements. A high-temperature, high-pressure dynamic mass transfer simulation system is then established. Simulated reservoir fluids—Tahe heavy oil and formation water containing 0.5 wt% nano-catalyst (1:1 v/v)—are introduced into the reactor chamber using an HPP-series temperature- and pressure-resistant mixer. The system operates at 140°C and 8 MPa, with weak reservoir-like shear conditions imposed by a reciprocating mechanism (0.5 Hz; shear rate γ = 15 s^{-1}) for 15 cycles. Throughout the process, real-time transmission light intensity data within the sapphire-windowed reactor are acquired at 50 ms intervals using an Ocean Optics HR4000 spectrometer. Based on Mie scattering theory, a quantitative inversion model correlates light intensity fluctuations with emulsion droplet

distributions. Simultaneously, high-speed micro-imaging captures fluid migration at the pore-throat scale. By coupling interfacial thermodynamic parameters with multiphase flow dynamics, this work reveals how active surface groups on the catalyst modulate interfacial film strength and emulsion stability at the oil-water interface, providing new insights into interfacial regulation mechanisms relevant to reservoir mass transfer processes.

Simulation Experiment of Heavy oil Reservoir Extraction

This study reports the development of a node-defective Ce/MOF-SDG catalyst via an integrated acid-etching and surface-functionalization strategy, achieving highly efficient catalytic viscosity reduction of heavy oil under mild conditions (140°C, 0.5 wt% catalyst). The catalyst exhibited outstanding performance, delivering a viscosity-reduction rate of 91.4% at a shear rate of 10 s^{-1} and enhancing oil-recovery efficiency to 87.78%—a 22.5% improvement compared with conventional water-alternating-gas (WAG) flooding. Comprehensive characterization and molecular simulations revealed that the catalytic enhancement originates from a synergistic electronic-structure modulation–interface engineering–multiphase catalysis framework. Acid etching generated abundant oxygen vacancies (≈35%) and coordinatively unsaturated Ce^{3+} sites (≈38.7%), which synergistically strengthened the Lewis acidity and redox capability of the active centers. Density-functional-theory calculations confirmed that these defects lowered the C–S bond-cleavage barrier to 5.1 kcal mol^{-1} through a distinctive bimetallic cooperative pathway, in which one Ce^{3+} species activates the target bond while another, stabilized by a μ_2-OH bridge, reduces the transition-state energy. Surface grafting of amphiphilic SDG polymers further augmented catalytic efficacy by improving dispersion (particle size reduced from 1.5–9 μm to 0.5–1 μm) and facilitating interfacial electron transfer, evidenced by bandgap narrowing from 2.8 to 1.7 eV. Product analyses demonstrated efficient conversion of heavy fractions into lighter species, with asphaltene and resin contents reduced by 9.56% and 2.66%, respectively, and the H/C ratio increased from 1.58 to 1.88. Elemental evaluation confirmed heteroatom removal efficiencies of 41.7% (S), 27.2% (N), and 23.8% (O), markedly improving oil quality. Notably, under mild shear (10 s^{-1}), Ce/MOF-SDG enabled heavy oil to transition into a flowable phase at ambient temperature, addressing the long-standing issue of wellbore transportability. The integrated defect-engineering–interface-design–reservoir-compatibility strategy established here provides fundamental insights and a scalable pathway for in-situ catalytic upgrading, defining a new paradigm for sustainable heavy-oil recovery and environmentally responsible energy production.

Supplementary Figures

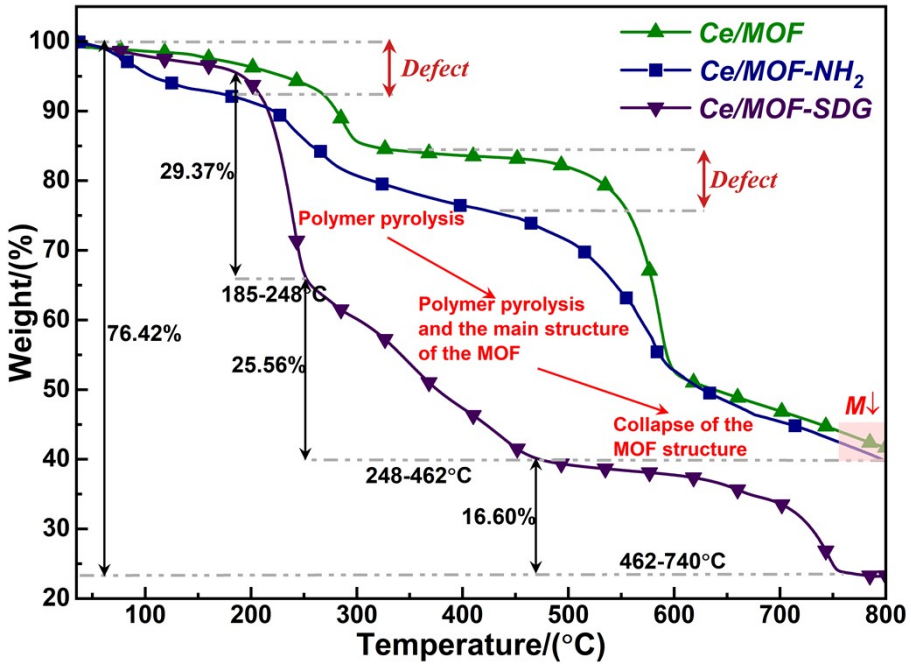

Fig. S1 Thermogravimetric (TGA) curve of the catalysts

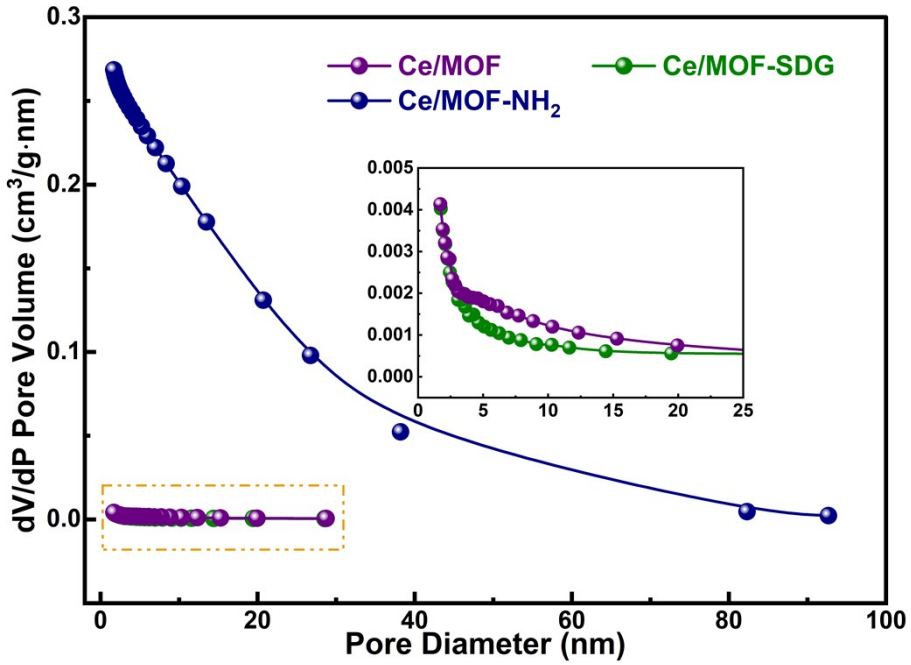

Fig. S2 Pore size distribution plot of the catalysts

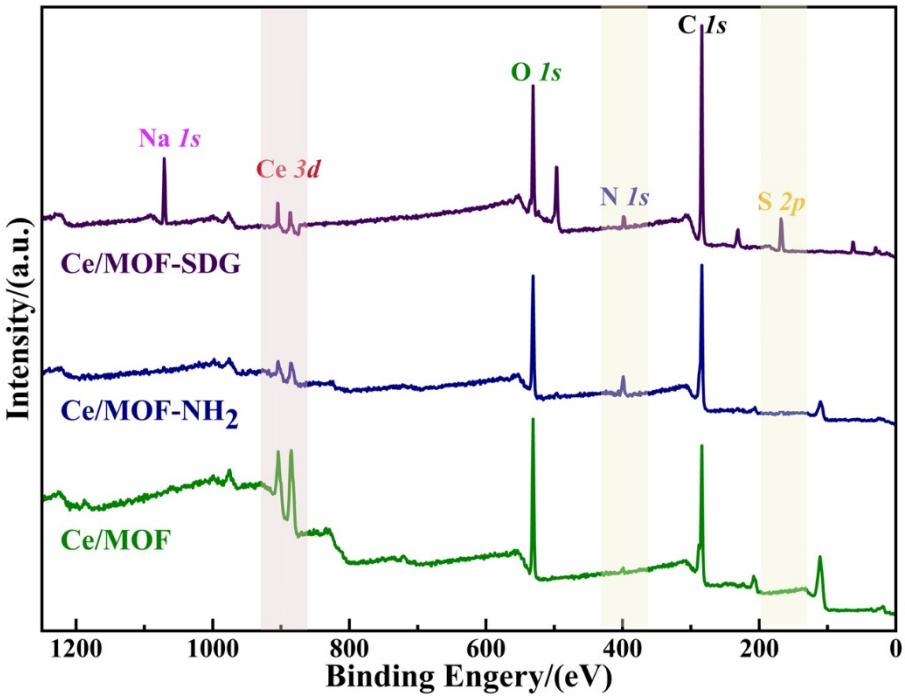

Fig. S3 XPS survey spectrum of the catalysts

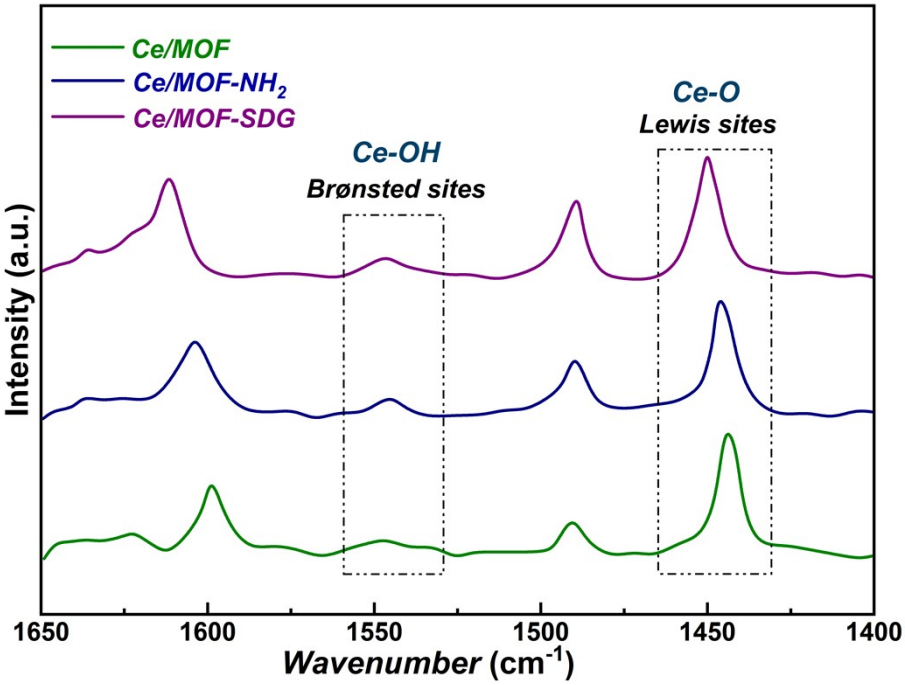

Fig. S4 Schematic diagram of pyridine-IR (Py-IR) of the catalyst

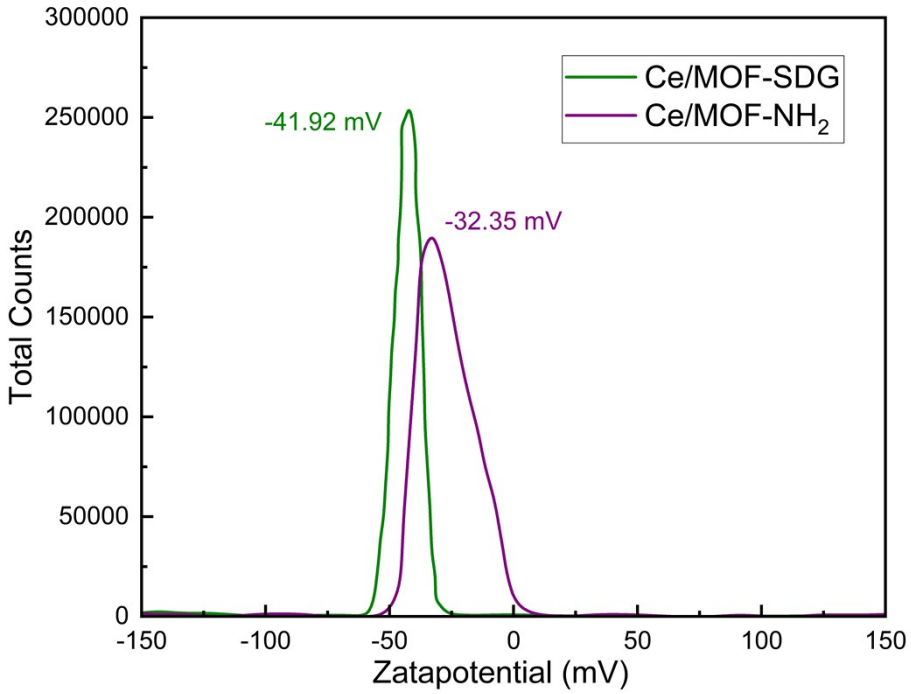

Fig. S5 Catalyst nanoparticle zeta potential analysis plot (0.5 wt% catalyst)

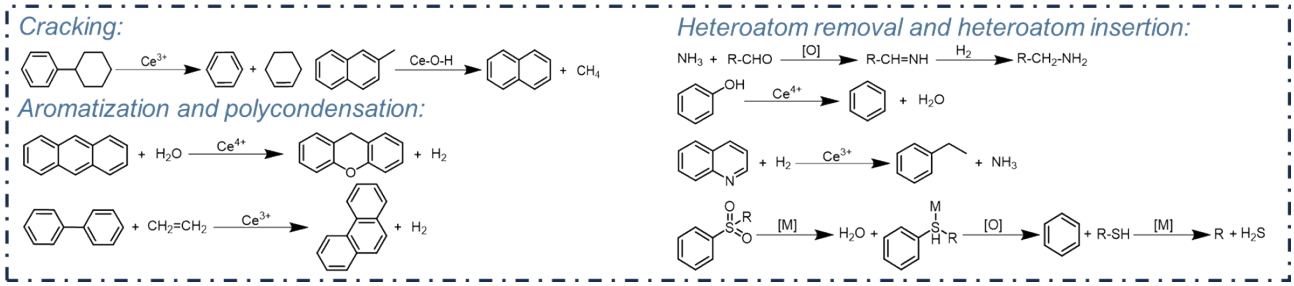

Fig. S6 Possible reactions during catalytic viscosity reduction of heavy oil

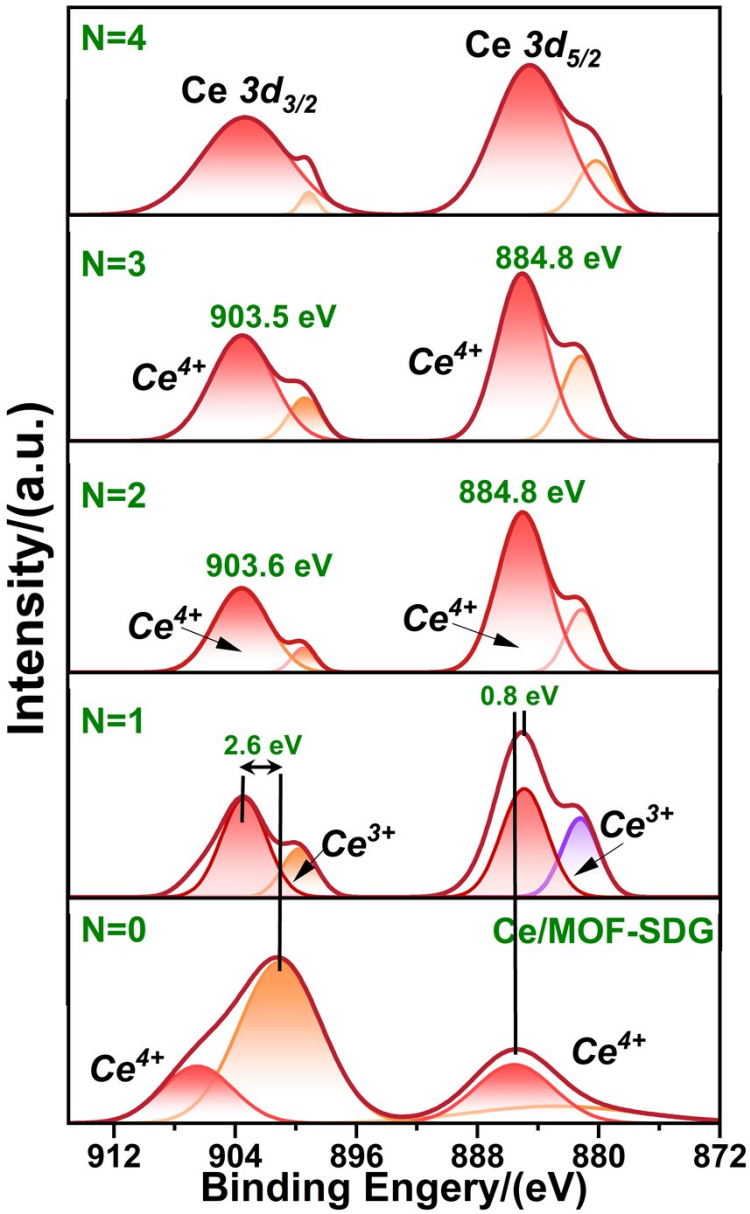

Fig. S7 Ce *3d* XPS spectra of fresh and recycled Ce/MOF-SDG catalysts over successive catalytic viscosity-reduction cycles

(The Ce *3d* XPS results indicate the presence of a pronounced mixed-valence Ce^{3+}/Ce^{4+} feature on the catalyst surface. The characteristic peaks at approximately 884.8 and 903.5–903.6 eV are mainly assigned to Ce^{4+}, while the shoulder peaks are attributed to Ce^{3+} species. Compared with the fresh catalyst, the samples collected in the initial recycling stage exhibit an enhanced Ce^{3+} signal accompanied by a slight binding-energy shift, indicating partial reduction of surface Ce sites during catalytic heavy-oil viscosity reduction. This suggests that the Ce^{3+}/Ce^{4+} redox couple participates in the reaction process and is closely associated with the formation or exposure of oxygen-vacancy-related active sites. Furthermore, with increasing cycle number, the main Ce *3d* peaks remain essentially unchanged, and no continuous significant peak shift or generation of new species is observed, indicating that the electronic structure of the Ce active centers is largely maintained during recycling without obvious irreversible damage. Therefore, the decline in catalytic activity is more likely attributable to reversible surface coverage or fouling by heavy components in the oil, rather than permanent loss of active sites or collapse of the catalyst framework.)

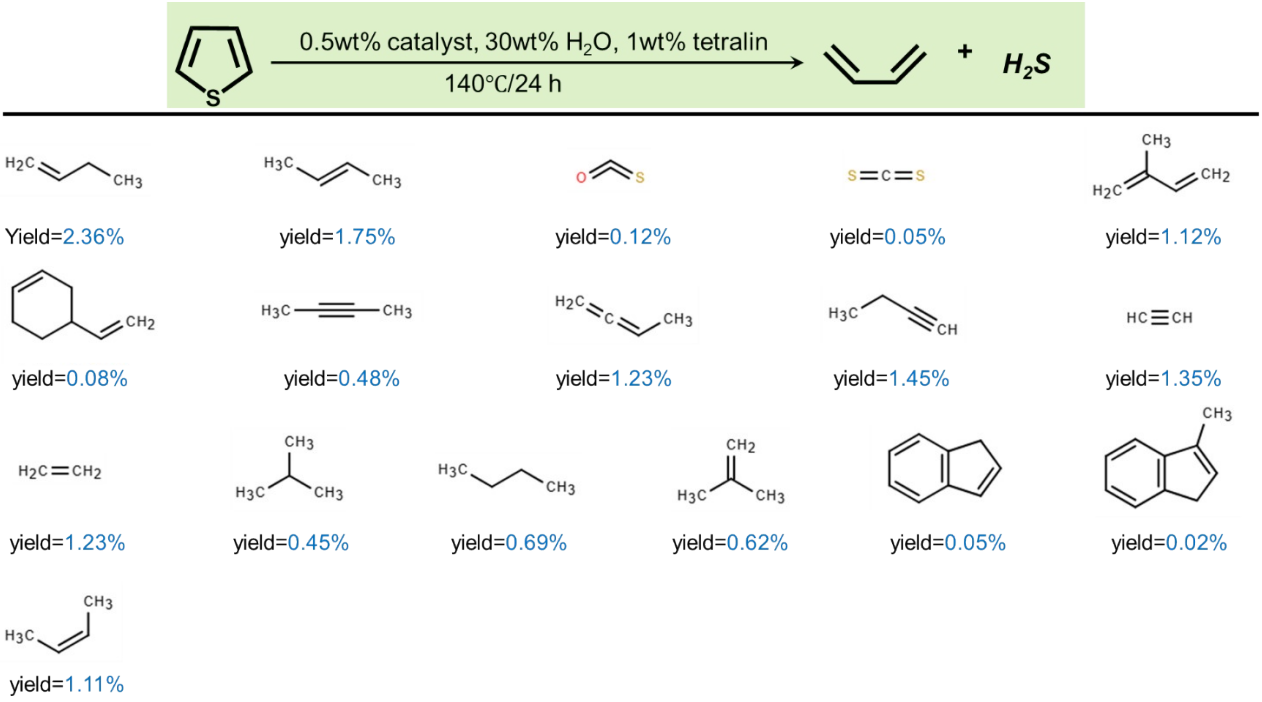

Fig. S8 Product distribution of thiophene catalytic reaction

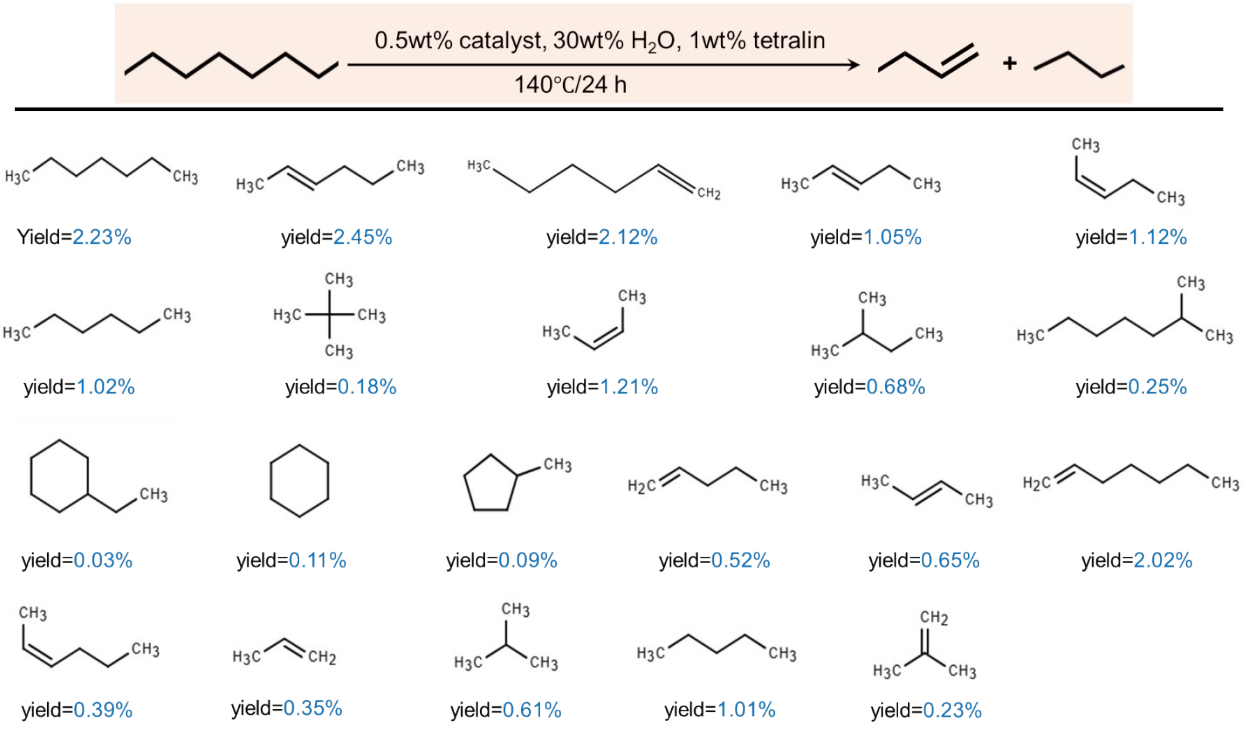

Fig. S9 Product distribution of n-octane catalytic reaction

Supplementary Tables

Supplementary Table S1. Main Properties of Crude Oil/%

Property	Analysis	Property	Analysis	Property	Analysis
Density ($g \cdot cm^{-3}$)	1.06 ± 0.02	O (%)	5.53 ± 0.03	Fe (ppm)	588±8.25
Saturated (%)	26.97 ± 0.58	N (%)	0.50 ± 0.02	Ni (ppm)	55±0.62
Aromatic (%)	14.68 ± 0.75	C (%)	84.42 ± 0.19	V (ppm)	291±3.19
Resin (%)	25.78 ± 0.58	S (%)	0.50 ± 0.04	Cu (ppm)	0.7±0.01
Asphaltene (%)	32.75 ± 0.89	H (%)	11.06 ± 0.04	Mg (ppm)	45±0.88

Supplementary Table S2. Content of ions and suspended matter in formation water samples of Tahe oilfield

Parameter	K^+	Ca^{2+}	Na^+	Mg^{2+}	Al^{3+}	Fe^{3+}	Cr^{6+}
Concentration (mg/L)	1.6×10^3	1.14×10^4	6.34×10^4	797	＜0.09	0.05	＜0.004
Parameter	V	Ni^{2+}	SO2- 4	Cl^-	Suspended solids	Total dissolved solids (TDS)	Total hardness (as $CaCO_3$)
Concentration (mg/L)	＜0.01	＜0.01	319	1.27×10^5	4	2.05×10^5	3.19×10^4